Verification of a Discrete Phase Model with Water-Particle Flow Experiments in a Tundish

Alexander Vakhrushev, Menguai Wu, Christian-Doppler Lab for Adv. Process Simulation of Solidification & Melting, University of Leoben, A-8700 Leoben, **Andreas Ludwig**, Chair of Simulation and Modeling of Metallurgical Processes, Department of Metallurgy, University of Leoben, A-8700 Leoben, **Gerhard Nitzl,** RHI AG, 1100 Vienna, Wienerbergstrasse 9, A-1100 Vienna, **Yong Tang, Gernot Hackl,** RHI AG, Technology Center, Magnesitstrasse 2, A-8700 Leoben, Austria
alexander.vakhrushev@unileoben.ac.at

Simulation of the melt flow, considered as a continuous phase, incorporating non-metallic inclusions and gas bubbles, represented as a discrete phase, is performed for the continuous casting tundish. A Discrete Phase Model (DPM) is employed in the Lagrangian frame of reference to track particles' motion whereas an Eulerian formulation is simultaneously used for the continuous phase. Different forces (viscous drag, lift force, buoyancy etc.) acting on the Lagrangian particles along their trajectories are taken into account as well as a stochastic behavior of the surrounding turbulent flow. The current study focuses on the verification of the numerical model and corresponding simulation results. Water modeling experiments were performed for a tundish flow with two different particle sizes. Being lighter than water, particles were captured at the framed top surface of the tundish and their measured distribution was used to verify the modeling results. The numerical simulations show good qualitative agreement with the experiments. The presented studies will help to improve the understanding of the transportation, separation and agglomeration mechanisms of non-metallic inclusions and gas bubbles in a turbulent melt flow. Their application in continuous casting will aim to increase inclusions removal and decrease defects formation in the final product.

1. Introduction

Numerical modeling of multiphase flow phenomena is of great importance for the simulation of the continuous casting process. Motion of non-metallic inclusions, engulfment of particles into the solidified shell, slag entrapment, flotation of injected gas bubbles etc. are points of interest for metallurgists. These tasks can be solved either by incorporating the full set of the Navier-Stokes equations for each simulated phase (Eulerian approach), or representing one of the phases as a dispersed (discrete) phase and track it in the Lagrangian frame of reference. Currently the most promising and effective methods in respect of computational time are the VOF method [1] as an Eulerian and the DPM method as a Lagrangian approach. However in the presented studies only the DPM method is employed and verified with a water particle flow experiment.

During modeling of solidification in continuous casting, the Lagrangian method has a huge advantage if it is exploited for the simulation of additional phases with the relatively small volume fraction (<10%). Here, a previously developed numerical model for the mold region [2], which was implemented in the open-source CFD package OpenFOAM® and showed a good performance, is applied for the tundish flow with the aim to perform its verification with water experiments.

The water experiments allow to qualitatively and quantitatively estimate the accuracy of the numerical results and to study the influence of the different forces, acting on the particles as well as their interaction with turbulence, described using a Discrete Random Walk (DRW) model [3].

2. Numerical model

The continuous media (water) represents an incompressible liquid with variable viscosity dependent on the local turbulent kinetic energy and its dissipation rate. The Finite Volume Method (FVM) is used with a so-called collocated or non-staggered variable arrangement (Rhie and Chow [4], Perić [5]), where all physical values share the same control volumes (CV), and all flux variables reside on the CV faces. A discrete phase, hereinafter referred to as "Lagrangian particles", is tracked within the Lagrangian framework.

2.1 Governing equations for the continuous phase

The Navier-Stokes equations with an assumption of the liquid being incompressible are used to simulate the liquid melt motion. The equation system consisting of the continuity and momentum conservation equations is

$$\nabla \cdot \mathbf{u} = 0\,, \tag{1}$$

$$\rho \frac{\partial \mathbf{u}}{\partial t} + \rho \nabla \cdot (\mathbf{u} \otimes \mathbf{u}) = -\nabla p + \nabla(\mu_{\text{eff}} \nabla \cdot \mathbf{u}) + \rho \vec{g} + \vec{S}_{\text{p}}\,. \tag{2}$$

It should be noted that the effective dynamic viscosity of the liquid μ_{eff} in the momentum conservation equation (2) is variable throughout the calculation domain due to turbulence. The presence of the discrete phase is considered in the source term $\vec{S}_{\text{p}}$, which represents the momentum exchange between the Lagrangian particles and the liquid flow. The estimation of its quantitative evaluation is described later.

In this study, a RANS turbulence approach is used based on $k-\varepsilon$ model, introduced by Launder and Sharma [6-7]. The realizable $k-\varepsilon$ model was employed [8], providing improved performance for flows involving boundary layers under strong pressure gradients and strong streamline curvatures. The governing equations for the turbulence are

$$\frac{\partial(\rho k)}{\partial t} + \nabla \cdot (\rho \vec{u} k) = \nabla \cdot \left(\left(\mu_{\ell} + \frac{\mu_{\text{t}}}{\text{Pr}_{\text{t,k}}} \right) \nabla k \right) + G - \rho \varepsilon, \tag{3}$$

$$\frac{\partial(\rho \varepsilon)}{\partial t} + \nabla \cdot (\rho \vec{u} \varepsilon) = \nabla \cdot \left(\left(\mu_{\ell} + \frac{\mu_{\text{t}}}{\text{Pr}_{\text{t},\varepsilon}} \right) \nabla \varepsilon \right) + \rho C_{1\varepsilon} S \varepsilon - C_{2\varepsilon} \rho \frac{\varepsilon^2}{k + \sqrt{\nu \varepsilon}}\,, \tag{4}$$

where μ_{ℓ} and μ_{t} are the molecular and the turbulent dynamic viscosity; ν is the laminar kinematic viscosity; $\text{Pr}_{\text{t,k}} = 1$, and $\text{Pr}_{\text{t},\varepsilon} = 1.3$ are the turbulent Prandtl numbers for k and ε respectively; G is the shear production of turbulence kinetic energy; $C_{1\varepsilon}$ and $C_{2\varepsilon}$ are the model constants.

In the momentum conservation equation, Eq.(2), the influence of turbulence is considered by an effective viscosity $\mu_{\text{eff}} = \mu_{\ell} + \mu_{\text{t}}$, where $\mu_{\text{t}} = \rho C_{\mu} k^2 / \varepsilon$ and $C_{\mu} = 0.09$.

2.2 Particle motion

To employ the DPM theory, a definition of the Lagrangian particle should be introduced. Hereinafter we consider a spherical particle with the diameter D_{P} and the density ρ_{P}. Thereby the mass of the particle is calculated as

$$m_{\text{P}} = \rho_{\text{P}} \frac{1}{6} \pi D_{\text{P}}^3. \tag{5}$$

Next, it is required to track the consecutive particles' trajectories through the simulation domain. Thereto each Lagrangian object is provided with its own position vector $\mathbf{x}_{\text{P}}$ in the Cartesian system of coordinates. To determine the particle's velocity $\mathbf{u}_{\text{P}}$ and the corresponding acceleration $\dot{\mathbf{u}}_{\text{P}}$, it is sufficient to compute the time derivatives of the trajectory vector $\mathbf{x}_{\text{P}}$ of the corresponding order

$$\dot{\mathbf{u}}_{\text{P}} = \ddot{\mathbf{x}}_{\text{P}}\,. \tag{6}$$

The calculation of the particle motion in the Lagrangian frame is based on Newton's Second Law. It binds the acceleration of the particle with the resulting forces, acting on it

$$m_{\text{P}} \dot{\mathbf{u}}_{\text{P}} = \sum \mathbf{F}_n\,, \tag{7}$$

where the sum of external forces $\sum \mathbf{F}_n$ originate from the influence from other Lagrangian particles as well as from the impact of the surrounding continuous media motion.

A number of forces are taken into account in the presented work. The simplification of the particle shape permits to utilize some analytical relations. For example, one of the most significant contributions comes from the particle viscous drag force. It is of complex nature and is based on the flow regime (either laminar or turbulent) around the Lagrangian particle. In general form one can formulate the drag force as

$$\mathbf{F}_{\mathrm{D}} = -m_{\mathrm{P}} \frac{\mathbf{u}_{\mathrm{P}} - \mathbf{u}}{\tau_{\mathrm{P}}}. \tag{8}$$

One can notice that the drag force (8) is based on the relative velocity $\mathbf{u}_{\mathrm{P}} - \mathbf{u}$ between the discrete and the continuous phases; τ_{P} represents the relaxation factor of the viscous drag. It is defined by the following relationship

$$\tau_{\mathrm{P}} = \frac{4}{3} \frac{\rho_{\mathrm{P}} D_{\mathrm{P}}}{\rho C_{\mathrm{D}} |\mathbf{u} - \mathbf{u}_{\mathrm{P}}|}. \tag{9}$$

The form, which is more appropriated for a numerical algorithm is obtained by substituting formulations (5) and (9) into relationship (8) for the drag force

$$\mathbf{F}_{\mathrm{D}} = \frac{1}{8} \pi \rho D_{\mathrm{P}}^2 C_{\mathrm{D}} |\mathbf{u} - \mathbf{u}_{\mathrm{P}}| (\mathbf{u} - \mathbf{u}_{\mathrm{P}}). \tag{10}$$

The important thing about the drag coefficient C_{D} is that it depends on the flow regime around the discrete particle (see Fig. 1).

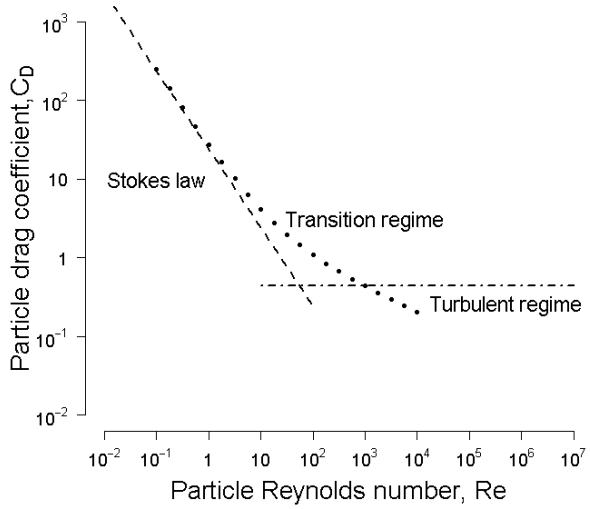

Fig. 1 Spherical particles drag law

Hereby, the drag law can be defined upon the relative particle Reynolds number being a counterpart of the flow Reynolds number

$$\mathrm{Re}_{\mathrm{P}} = \frac{\rho D_{\mathrm{P}} |\mathbf{u} - \mathbf{u}_{\mathrm{P}}|}{\mu}. \tag{11}$$

In the presented investigations the drag coefficient corresponds to the Schiller-Naumann approximation [9]

$$C_{\mathrm{D}} = \begin{cases} \dfrac{24}{\mathrm{Re}_{\mathrm{P}}}, & \text{if } \mathrm{Re}_{\mathrm{P}} \le 0.1; \\ \dfrac{24}{\mathrm{Re}_{\mathrm{P}}} \left(1 + 0.15\, \mathrm{Re}_{\mathrm{P}}^{0.687}\right), & \text{if } 0.1 \le \mathrm{Re}_{\mathrm{P}} \le 10^3; \\ 0.44, & \text{if } \mathrm{Re}_{\mathrm{P}} > 10^3. \end{cases} \tag{12}$$

In general, it was shown, that the particle relaxation time is depended upon the particle relative Reynolds number. In the case of the Stokesian drag, where $\mathrm{Re_P}$ is rather small ($\ll 1$) and drag coefficient C_D, according to (12), is equal to $\frac{24}{\mathrm{Re_P}}$. Thus particle relaxation time is dependent upon only the media properties

$$\tau_\mathrm{P} = \frac{\rho_\mathrm{P} D_\mathrm{P}^2}{18\mu}. \tag{13}$$

Further to the drag force, the gravitational force $\mathbf{F}_\mathrm{B}$, the lift force $\mathbf{F}_\mathrm{L}$, the virtual mass force $\mathbf{F}_\mathrm{V}$, and the pressure and stress gradient force $\mathbf{F}_\mathrm{P}$ were implemented for the nonmetallic inclusions motion in the tundish and the CC mold.

The gravitational or buoyancy force can be described as

$$\mathbf{F}_\mathrm{B} = \frac{1}{6}\pi D_\mathrm{P}^3(\rho_\mathrm{P} - \rho)\mathbf{g}. \tag{14}$$

One can notice, that $\mathbf{F}_\mathrm{B}$ is stronger with the growing difference between the particle and the liquid density, and its effect is even greater with the increasing diameter of the discrete object. Thereby, preliminary one can state that the buoyancy force will dominate in the case of gas bubbles motion.

The virtual mass force is required to accelerate and displace the fluid mass surrounding a particle when it moves through it. This leads to an additional drag. The virtual mass force is important if the density of the surrounding melt is bigger than the density of the particle. This is the case for steel as the melt has the twice higher density than the non-metallic inclusions. If argon gas and steel are compared, the difference is even bigger (10^5). The formula for the virtual mass force in the particle force balance is [10]

$$\mathbf{F}_\mathrm{V} = \frac{\rho\pi D_\mathrm{P}^3}{12}\frac{\mathrm{d}}{\mathrm{dt}}(\mathbf{u} - \mathbf{u}_\mathrm{P}). \tag{15}$$

Lift force on a particle arises due to particle rotation in a velocity gradient. A higher velocity on one side of a particle gives rise to a low pressure and on the other side due to a lower velocity to a high pressure. This force tends the particle to move into the direction of the smaller pressure. Saffman [11] derived an expression for the lift force on solid spherical particles in an unbounded linear shear flow. Saffman's formula is based on the conditions that the relative particle Reynolds number $\mathrm{Re_P}$ is much lower than the shear Reynolds number $\mathrm{Re_G}$, which is defined as

$$\mathrm{Re_G} = \frac{\rho D_\mathrm{P}^2}{\mu}|\dot{\gamma}|, \tag{16}$$

where $\dot{\gamma}$ represents the shear rate in fluid. Thus

$$\mathbf{F}_{\mathrm{L(Saff)}} = \frac{9}{\pi}\frac{D_\mathrm{P}}{2}\mu(\mathbf{u} - \mathbf{u}_\mathrm{P})\sqrt{\mathrm{Re_G}}\,\mathrm{sgn}(\dot{\gamma}). \tag{17}$$

Wang and McLaughlin extended the force to allow the relative particle Reynolds number to exceed the shear Reynolds number by implementing a correction factor $J(\beta) = \frac{\mathbf{F}_\mathrm{L}}{\mathbf{F}_{\mathrm{L(Saff)}}}$ [12],

$$J = \begin{cases} -32\pi^2\beta^5 \ln\beta^{-2}, & \beta < 0.1; \\ 0.6765\left[1 + \tanh(2.5\log\beta + 0.191\right]\cdot \\ \cdot\left\{0.667 + \tanh[6(\beta - 0.32)]\right\} & 0.1. \le \beta \le 20; \end{cases}. \tag{18}$$

where $\beta = \frac{\sqrt{\mathrm{Re_G}}}{\mathrm{Re_P}}$.

An additional force arises due to the pressure and stress gradient in the fluid. It is derived from the momentum conservation equation as follows [3]

$$\mathbf{F}_{\mathrm{P}} = -\frac{\pi D_{\mathrm{P}}^3}{6}\rho u_{p_i}\frac{\partial u_i}{\partial x_i}. \tag{19}$$

As it was shown previously [13] that for continuous casting the motion of inclusions is mainly governed by the drag and the buoyancy forces. The influence of the lift force is especially important in areas with the strong velocity gradient in shear layer flows near walls, and its action is concurrent to the flow direction.

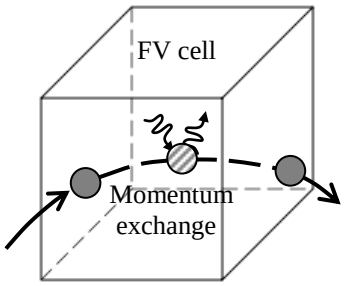

Fig. 2 Interaction of Lagrangian particles with continuous phase

As shown in Fig. 2, to couple the momentum in both phases, the momentum exchange is determined in each finite volume of the numerical mesh being used for the continuous phase. For the mesh element with the index k and of the volume V_k the momentum exchange rate is calculated as

$$\mathbf{S}_P^k = \frac{1}{V_k \Delta t}\sum_{\mathrm{P}} m_{\mathrm{P}}\left[\left(\mathbf{u}_{\mathrm{P}}\right)_{in}^k - \left(\mathbf{u}_{\mathrm{P}}\right)_{out}^k\right]. \tag{20}$$

To represent the particle / solid wall interaction the bouncing model is defined by the restitution factor ε_{wall} and the wall friction coefficient μ_{wall}. Splitting the particle velocity vector into the normal $\mathbf{u}_{\mathrm{P}}^{\mathbf{n}}$ and the tangential $\mathbf{u}_{\mathrm{P}}^{\boldsymbol{\tau}}$ components, one can achieve a new particle velocity $\tilde{\mathbf{u}}_{\mathrm{P}}$ after its interaction with the firm surface

$$\begin{cases} \tilde{\mathbf{u}}_{\mathrm{P}} = \tilde{\mathbf{u}}_{\mathrm{P}}^{\mathbf{n}} + \tilde{\mathbf{u}}_{\mathrm{P}}^{\boldsymbol{\tau}}, \\ \tilde{\mathbf{u}}_{\mathrm{P}}^{\mathbf{n}} = -\varepsilon_{wall}\mathbf{u}_{\mathrm{P}}^{\mathbf{n}}, \\ \tilde{\mathbf{u}}_{\mathrm{P}}^{\boldsymbol{\tau}} = \left(1-\mu_{wall}\right)\mathbf{u}_{\mathrm{P}}^{\boldsymbol{\tau}}. \end{cases} \tag{21}$$

The complexity of the discrete phase interaction with turbulent eddies of the viscous flow is taken into account by the following stochastic approach. The typical trajectory of the small particle / gas bubble inside the turbulent eddy is represented in Fig. 3. To introduce such a behavior of the Lagrangian particle in the presented model a Discrete Random Walk model can be employed [3,14,15]. Its main assumptions concern the introduction of the so-called "eddy life time" t_{eddy} and "crossing time" t_{cross} scales as follows

$$\begin{cases} t_{eddy} = -0{,}15\dfrac{k}{\varepsilon}\log r, \\ t_{cross} = -\tau_{\mathrm{P}}\ln\left[1-\left(\dfrac{L_{eddy}}{\tau_{\mathrm{P}}\left|\mathbf{u}-\mathbf{u}_{\mathrm{P}}\right|}\right)\right], \\ L_{eddy} = c_{\mu}^{1/2}\dfrac{k^{3/2}}{\varepsilon}, \\ t_{\mathrm{P}}^{DRW} = \min\left\{t_{eddy}, t_{cross}\right\}. \end{cases} \tag{22}$$

Here r is a uniform random number between 0 and 1. The variable t_{eddy} describes the characteristic time within which the eddy can exist until it is dissipated, whereas t_{cross} defines the time interval which would be sufficient for the discrete phase object to cross the eddy. Both parameters are based on the local turbulence parameters.

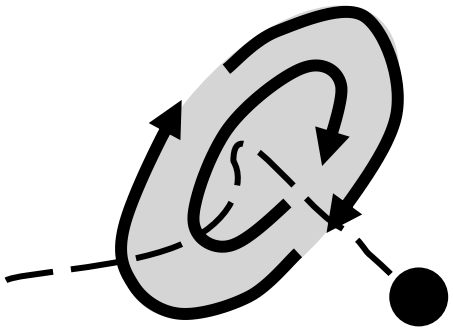

Fig. 3 Schematic particle trajectory due to interaction with a turbulent eddy

The instant velocity of the continuous media at a local point represents the sum of the mean and fluctuating components

$$\mathbf{u} = \overline{\mathbf{u}} + \mathbf{u}', \tag{23}$$

The stochastic part of the instantaneous velocity vector is

$$\mathbf{u}' = \zeta\sqrt{\frac{2k}{3}}\ . \tag{24}$$

Here, ζ is a normally distributed random number. The adjusted drag force acting on the particle can be written in the form

$$\mathbf{F}_{\mathrm{D}} = \frac{1}{8}\pi\rho D_{\mathrm{P}}^2 C_{\mathrm{D}}\left|\mathbf{u}-\mathbf{u}_{\mathrm{P}}\right|\left(\mathbf{u}+\mathbf{u}'-\mathbf{u}_{\mathrm{P}}\right). \tag{25}$$

To include the turbulence influence in the simulation algorithm a random velocity component $\mathbf{u}'$ is calculated based on Eq. (24) to be used in Eq. (25) for the modified drag law. The characteristic time when $\mathbf{u}'$ acts on a particle is the smallest value between eddy life and crossing time.

2.3 Solution procedure for a coupled model

After assembling the numerical model we end up with a system of partially differential equations (PDEs) with several non-linear terms supplemented with the ordinary differential equations for Lagrangian particles. As a very next step it is important to perform numerical coupling between the different parts of the model. For large time-step transient calculations the PIMPLE algorithm represents a merged version of the widely used SIMPLE and PISO methods for pressure-velocity coupling [16-17]. Internal iteration loops are used with underelaxations being applied either for the model variables or for the matrices of the linear equation systems to be solved. The iteration process stabilizes the numerical solution and enables the use of time-step values which results in Courant numbers $Co >> 1$.

Based on the fluid flow field the new trajectories for the particles are calculated. After that an updated sink term is introduced in the momentum equation, and the liquid flow is simulated again. Fig. 4 shows a flow chart of the flow / Lagrangian particles solver as a generalization of the described algorithm. It should be noted that all internal loops of the solution algorithm are executed until either the global convergence criterion is fulfilled (for a fully transient solution) or the prescribed number of steps is executed (if steady state is targeted).

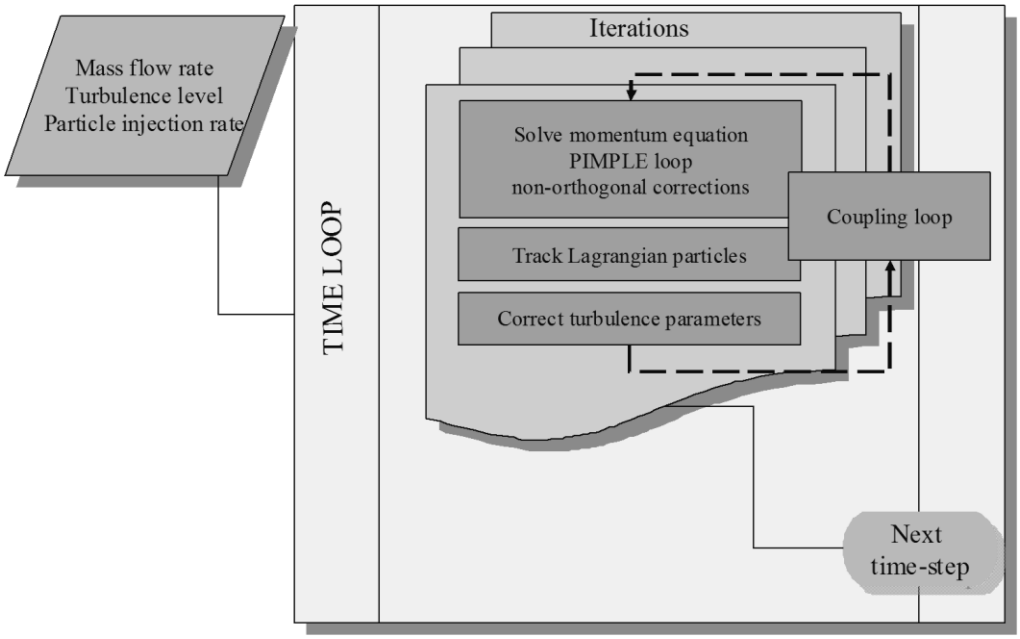

Fig. 4 Flow chart of the designed solver

A vector-tensor form of the equations is used in the OpenFOAM® development environment [18] using the advantages of the object-oriented programming. All drag and force models as well as the boundary conditions are implemented by the authors in an in-house source code.

A collection of the corresponding solvers, developed in cooperation of the authors group, is called OPENCAST and will be referred to later during the results discussion.

3. Experimental procedure

To verify the numerical results and to perform different parameter studies water particle flow experiments were performed at the laboratory of voestalpine Stahl (Linz, Austria). This section briefly describes the experimental setup and the methodology of the performed measurements.

3.1 Laboratory experiment setup

The particle water flow experiments include spherical tracers being injected through a shroud with the water jet into a tundish model. The transparent walls of the tundish allow recording the particles motion inside the stream. However, it is unrealistic to track the trajectory of each individual object based on camera data in order to quantify the numerical results. Thereby, an immersed wooden frame was mounted on top of the tundish to capture the floating particles. Of course, a slight transversal motion of the tracers was observed between the cells but it had no dramatic influence on the final measured distribution.

After such an experiment was finished, particles were collected from the cage frames as well as from the outflow of the system. Knowing the initial mass of the used tracers, it was thus possible to estimate a distribution of the weighted particles along the free surface.

Tab. 1 Particle properties and water flow parameters

Diameter (mm)	Density (kg/m^3)	Particle mass flow rate (kg/s)	Water flow rate (m^3/min)	Injection time (s)
3.5	950	0.0581	0.426	32
0.285	850	0.0581	0.426	16

The particle diameter used in the experiment, the particle mass flow rate and the water flow rate are summarized in Tab. 1. It should be mentioned that the particle diameters reveal some scatter whereas the size of the Lagrangian particles in the numerical simulations is the somehow averaged value of the experimental distribution.

3.2 Numerical simulation settings

As it is described in the previous section, the averaged experiment parameters are used for the numerical modeling of the particles flow in a tundish (Tab. 1). Fig. 5 (a) shows the simulation domain with the tracked stream lines showing the complicity of the turbulent flow inside the tundish. To perform a quantitative comparison with the laboratory experiment the top part of the boundary in the simulation is split into the same arrangement as the experimental frame (Fig. 5 (b)), where each captured tracer is counted and recorded.

A transient simulation includes turbulent flow modeling along with tracking of discrete particles. All forces, been described in Sec. 2.2, are taken into account as well the DRW model for the particles separation due to turbulence. A numerical turbulence models were previously tested and verified with the experimental data by Odenthal and Javurek [19-20] and were approved for the tundish flow simulations.

A series of simulation runs were performed to study the influence of the different forces on the final distribution of the captured particles. The results of the comparison with experimental findings and its analysis are presented in the next section.

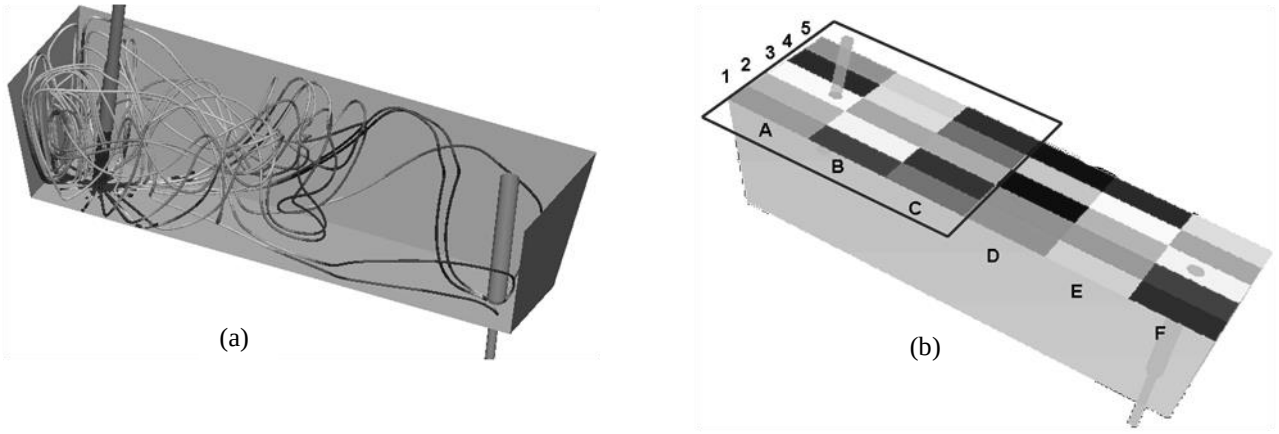

Fig. 5 Particle simulation in a tundish: (a) turbulent flow stream-lines
and (b) patching the top surface to count the captured particles

4. Results and Discussion

At the final stage of the water modeling experiments it was observed that bigger particles with diameter 3.5 mm are significantly separated. On the contrary, smaller particles look more like a continuous layer or foam on the top of a tundush. Just a simple comparison of the particle sizes shows that big tracers have a volume 1852 times larger $\left(\frac{d_{big}}{d_{small}}\right)^3$ than the small ones. Thereby, only the bigger particles are considered for the simulations presented in the current study. For the proper and more effective modeling of the smaller particles a cloud theory should be appropriate to implemented in the CFD solver.

Next, different simulations with the developed coupled solver were performed. An instant picture of the particles separated in the turbulent flow is presented in Fig. 6. It corresponds to the moment when the injection process is completed and all traced particles are in the simulation domain.

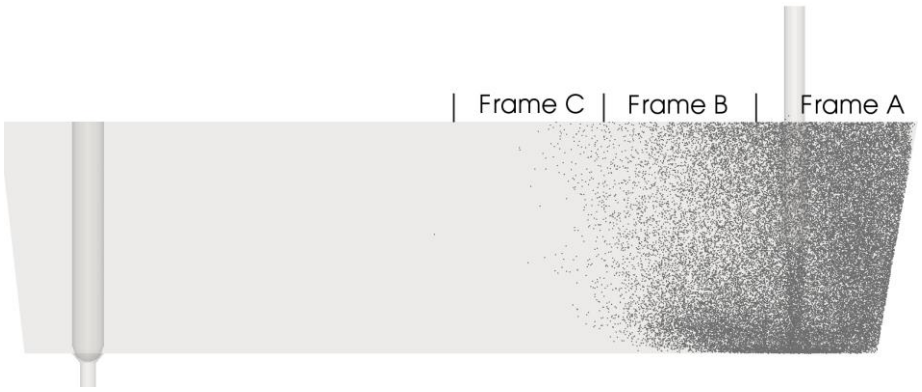

Fig 6 Simulation results after particles injection is finished

As it was mentioned before, the top surface of the simulation domain (representing the slag layer) was divided to the corresponding number of patches exactly conforming to the location of the cells of the capturing frame in the experiment.

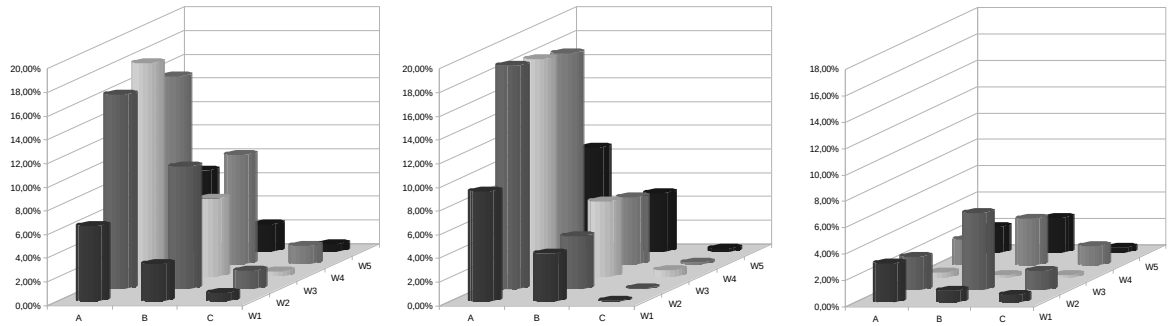

(a) experiment (b) OPENCAST (c) experiment vs. OPENCAST

Fig. 7 Comparison of the experimental data with the simulated ones: total amount of the particles being captured (a) in the experiment, (b) predicted by the simulation; (c) difference between acquired data sets

The distribution of the particles captured at the top surface during the experiments and in the computer simulations with the OPENCAST solver (Fig. 7) was compared. Obviously, the OPENCAST simulation shows good agreement with the experiment along the tundish walls. However in the central part the predictions of the numerical model give the largest differences if compared to the experiments. The fundamentals of the simulation results deviation from the experimental observation can be explained either by the model simplifications, or by the numerical treatment of the forces. The results of the single and cumulative effects of the different particle forces will be presented in the consecutive paper.

5. Conclusions

A complex model for the simulation of the discrete phase is developed and verified with the water modeling experiment. The numerical simulation showed good qualitative agreement with the experimental data.

Developed model can be applied for the continuous casting simulations in the tundish, submerged entry nozzle and mold regions. A cloud model should complement designed solvers to be more suitable for the systems with a huge amount of particles to be tracked. In this case it is better to substitute the effect of a single particle with an impact of a so called parcel, representing a collection of the smaller objects with some distribution inside the volume of the parcel.

In the conclusion it should be mentioned, that the results and the numerical model, presented in this study, are quite important for the fundamental and practical applications.

Acknowledgement

The financial support by RHI AG, the Austrian Federal Ministry of Economy, Family and Youth and the National Foundation for Research, Technology and Development in the framework of Christian-Doppler Laboratory for Advanced Process Simulation of Solidification and Melting is gratefully acknowledged. The authors acknowledge the voestalpine Stahl (Linz) for the support and performance of the water modeling experiment.

References

[1] HIRT, C. W.; NICHOLS, B. D. Volume of fluid (VOF) method for the dynamics of free boundaries; J. Comp. Physics, 1981, vol. 39, Issue 1, P. 201-225

[2] VAKHRUSHEV A., LUDWIG A., WU M., TANG Y., NITZL G., HACKL G. Modeling of Nonmetallic Inclusions and Gas Bubbles motion in Continuous Caster. 4th Int. Conf. Simulation and Modeling in Metallurgical Processes in Steelmaking (STEELSIM 2011) Düsseldorf, Germany, June 27 – July 01 (2011) S17.1-8.

[3] FLUENT 6.3 User's Guide, Fluent Inc., 2006

[4] RHIE, C. M.; CHOW, W. L. A numerical study of the turbulent flow past an isolated airfoil with trailing edge separation; 3rd Joint Thermophysics, Fluids, Plasma and Heat Transfer Conference, St. Louis, Missouri, 1982

[5] PERIĆ, M. A Finite Volume method for the prediction of three-dimensional fluid flow in complex ducts; PhD thesis, Imperial College, University of London, 1985

[6] JONES, W. P.; LAUNDER, B. E. The Prediction of Laminarization with a Two-Equation Model of Turbulence; Int. J. Heat and Mass Transfer, 1973, vol. 15, P. 301-314

[7] LAUNDER, B. E.; SHARMA, B. I. Application of the Energy Dissipation Model of Turbulence to the Calculation of Flow Near a Spinning Disc; Let. Heat and Mass Transfer, 1974, vol. 1, N 2, P. 131-138

[8] SHIH, T. H., LIOU, W. W., SHABBIR, A., YANG, Z, ZHU, J. A new k-є eddy viscosity model for high Reynolds number turbulent flows, Computers & Fluids, Volume 24, Issue 3, March 1995, P. 227-238

[9] SCHILLER, L.; NAUMANN, Z. Über die grundlegenden Berechnungen bei der Schwerkrafttaufbereitung (in Germany); Ver. Deut. Ing., 77, 1933, P. 318-320

[10] CROWE, C.; SOMMERFELD, M.; TSUJI, Y. Multiphase Flows with Droplets and Particles; CRC Press LLC, 1998

[11] SAFFMAN, P. G. The lift on a small sphere in a slow shear flow; J. Fluid Mech., 1965, vol. 22, P. 385

[12] WANG, Q.; SQUIRES, K. D.; CHEN, M.; MCLAUGHLIN, J. B. On the Role of the Lift Force in Turbulence Simulations of Particle Deposition; Int. J. Multiphase Flow, 1997, 23 (4), P. 749-763

[13] YUAN, Q. Transient Study of Turbulent Flow and Particle Transport During Continuous Casting of Steel Slabs; Ph.D. thesis, M & I Eng. Univ. of Illinois, Urbana, IL, 2004

[14] GRAHAM, D. I.; JAMES, P. W. Turbulent dispersion of particles using eddy interaction models; Int. J. Multiphase Flow, 1996, vol. 22, Issue 1, P. 157-175

[15] GRAHAM, D. I. On the inertia effect in eddy interaction models; Int. J. Multiphase Flow, 1996, vol. 22, Issue 1, P. 177-184

[16] PATANKAR, S. V. Numerical Heat Transfer and Fluid Flow; Taylor & Francis, USA, 1980

[17] FERZIGER, J. H.; PERIC, M. Computational Methods for Fluid Dynamics; Springer, Germany, 2002

[18] WELLER, H. G.; TABOR, G.; JASAK, H.; FUREBY, C. A tensorial approach to CFD using object orientated techniques; Computers in Physics, 1998, vol. 12, P. 620–631

[19] ODENTHAL H.-J., JAVUREK M., KIRSCHEN M., CFD Benchmark for a Single Strand Tundish (Part I). Steel research international Volume 80, Issue 4, pp. 264–274, April 2009

[20] ODENTHAL H.-J., JAVUREK M., KIRSCHEN M., VOGL N., CFD Benchmark for a Single Strand Tundish (Part II). Steel research international Volume 81, Issue 7, pp. 529–541, July 2010